Journal of the European Ceramic Society 21 (2001) 569–580

www.elsevier.com/locate/jeurceramsoc

Microstructural stability and room temperature mechanical properties of the Nextel 720 fibre

F. Deléglise, M.H. Berger, D. Jeulin, A.R. Bunsell *

Ecole des Mines de Paris, Centre des Matériaux, BP 87, Evry Cedex, France

Received 16 March 2000; received in revised form 13 July 2000; accepted 31 July 2000

Abstract

The microstructure and tensile properties of the as-received and heat-treated Nextel 720 fibre have been studied. During its fabrication the Nextel 720 fibre is pyrolysed at a temperature lower than 1400°C for a very short time which does not allow the microstructure to be stabilised. A pseudo-tetragonal metastable alumina rich mullite is formed which crystallises in the form of mosaic grains containing low angle boundaries. These mosaic grains enclose some rounded and elongated α-alumina grains. The evolution of the mullite to the stable orthorhombic symmetry is seen from 1200°C for post heat treatments lasting several hours. For longer heat treatments at 1200°C or at 1300°C and higher temperatures, the mosaic grains begin to recrystallise into single grains and the alumina rejected from the mullite contributes to the growth of elongated α-alumina grains which suggests diffusion through an intergranular liquid silicate phase. At 1400°C the mullite has the 3:2 composition and after 24 h the growth of the elongated α-alumina grains leads to a reduction of the room temperature tensile strengths. The α-alumina creation coupled to the phase transformation and dissolution of mullite leads to an increase of the Young's modulus after heat treatments from 1200°C.

Keywords: Al_2O_3; Fibres; Mechanical properties; Microstructure-final; Mullite

1. Introduction

The applications of ceramic matrix composites require reinforcement materials with long term high temperature chemical stability in oxidising atmospheres above 1300°C and ideally above 1500°C. SiC fibres have excellent mechanical properties at temperatures of up to 1500°C in inert atmospheres. However, at temperatures above 1200°C they begin to suffer from oxidation which ultimately restricts their use to a maximum temperature of around 1400°C. Oxide based fibres do offer an excellent chemical stability in air to higher temperatures. The 3M Nextel 720 fibre, which is the latest of a series of fibres produced by 3M based on alumina and mullite is the commercial oxide fibre with the most promising creep properties. The aim of this paper is to study the microstructure and mechanical properties of this fibre and the influence of high temperature treatments on the microstructure and on the residual mechanical properties.

2. Material

The 12.5 μm diameter Nextel 720 mullite-alumina fibre produced by 3M is composed of 85% Al_2O_3 and 15% SiO_2 by weight. The room temperature single filament strength announced by the manufacturer is 2100 MPa at a gauge length of 25 mm and its Young's modulus is 250 GPa. This fibre has an original microstructure consisting of mosaic and elongated grains.[1]

3. Experimental procedure

The microstructures and mechanical properties at room temperature have been investigated on as-received and heat treated fibres. Great care was taken not to contaminate the fibres during handling. Contact with the skin was avoided by the use of surgical gloves.

* Corresponding author. Tel.: +33-1-60-76-3015; fax: +33-1-60-76-3150.

E-mail address: anthony.bunsell@mat.ensmp.fr (A.R. Bunsell).

0955-2219/01/$ - see front matter
PII: S0955-2219(00)00249-1

The diameters of the fibres were measured prior to each test using a Watson ocular mounted on an optical microscope allowing a resolution of 0.5 μm.[2] The external surfaces of the fibres as well as their fracture surfaces were observed using a LEO DSM 982 Gemini FEG SEM at acceleration voltages between 1 and 3 kV. The microstructures and the effects on heat-treatments were investigated using a PHILIPS EM 430 TEM-STEM (300 kV). A CM200 FEG-TEM (200 kV) has also been used at the US National Center for Electron Microscopy, Lawrence Berkeley National Laboratory, University of California. Thin foils were obtained using a method described elsewhere.[3] Heat treatments were performed in a $MoSi_2$ resistance furnace. An X-ray diffractometer Siemens D500 was used to analyze the different phases and the influence of heat treatments on the crystal structures. The radiation corresponds to the $K_{\alpha 1}$ line of cobalt ($\lambda = 0.1789$ nm). Semi-quantitative and quantitative microanalysis was performed using EDS and WDS techniques.

Tensile tests have been carried out on as-received and heat-treated fibres. Single filaments were tested on an horizontal tensile machine with a maximum displacement speed of 1.5 mm/s and a load sensitivity of 0.1 g.[4]

4. Results

4.1. Composition and microstructure of the as-received fibre

The external appearance of the Nextel 720 fibre is shown in Fig. 1. The fibre has a circular cross-section, with a diameter of 12.5±0.5 μm. The fibre section appeared smoother and less granular than that of pure alpha alumina fibres but exhibited zones of about 0.5 μm in size with irregular contours.

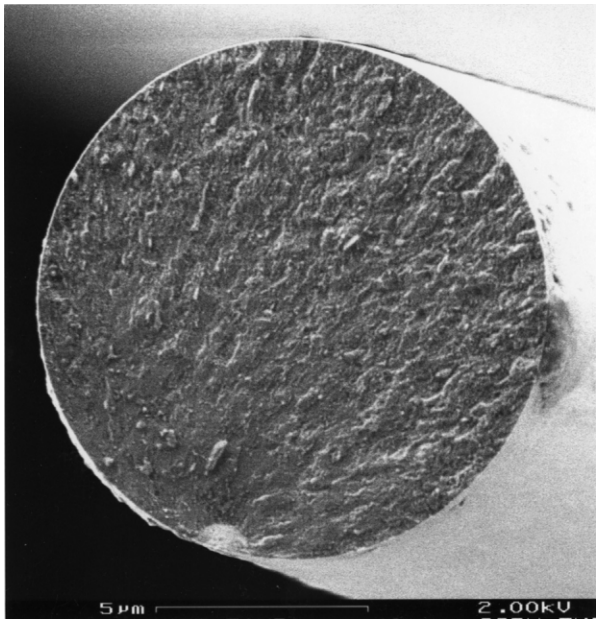

Fig. 1. Fracture morphology of the as-received fibre.

XRD spectra analysis revealed the presence of α-alumina peaks plus a set of peaks close to those of the orthorhombic stoichiometric 3:2 mullite (ASTM 15-776) as seen in Table 1. However, it was observed that for each of the hkl and khl diffracting planes the corresponding peaks were overlapping as can be seen on Fig. 2 for the 210/120 couple.

WDS analyses revealed the presence of 0.3% Fe in weight and few ppm of Na, K and Cl in the bulk of the fibre. The surface presented randomly distributed inclusions rich in Ca, Na, Mg and Cl and K as shown in Fig. 3.

Dark diffracting areas with wavy contours with an average size of 450 nm can be observed in the TEM pictures shown in Fig. 4 and their structure are revealed in the HRTEM images of Fig. 5. They correspond to aggregates of mullite grains each of a few tens of nanometers in size and showing close cristallographical orientations. When tilting an area of the sample over a large range of orientations (Fig. 6) it became apparent that each part of this area showed an aggregate for a given angle of incidence, the contour of which followed the neighbouring aggregates. These aggregates, or mosaic grains, were isotropic and larger than the thickness of the thin foil (about 50 nm) so that we can conclude that

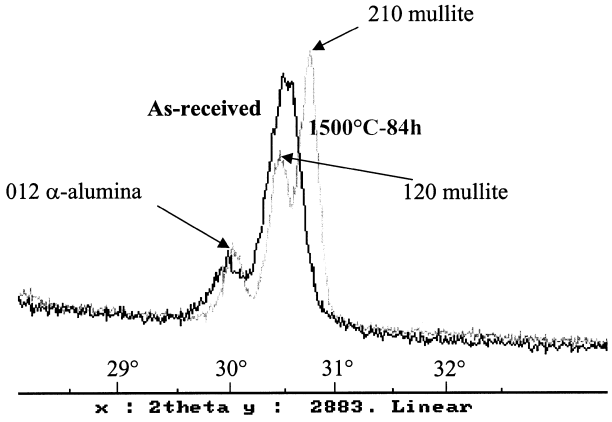

Fig. 2. Part of the XRD spectra showing, for the as received fibre that the 210 and 120 mullite peaks were overlapping whereas after heat-treatment for 84 h at 1500°C splitting of the 120/210 occurred.

Table 1
Position of the X-ray 120, 210, 001 diffraction peaks measured with the as received fibre and after different heat-treatments

Peaks hkl	ASTM 15-776	As-received	1200°C, 5 h	1400°C, 24 h	1500°C, 84 h
120 d (Å)	3.428	3.412	3.403	3.411	3.407
210 d (Å)	3.390	3.391	3.381	3.377	3.370
001 d (Å)	2.886	2.880	2.873	2.873	2.866

the whole fibre was composed of these adjoining mosaic grains. The mullite aggregates enclosed α-alumina in the form of spherical particles of 50 nm on average and ranging from 20 to 100 nm and or elongated grains of 100 nm on average, ranging from 50 to 300 nm in length with aspect ratios of up to 6. These elongated grains were preferentially oriented towards the fibre axis and grew perpendicularly to the [0001] axis as illustrated in Fig. 7. Orientation relationships have been revealed between mullite and α-alumina grains as shown in Fig. 8. No intergranular amorphous phases were detected in the fibre.

4.2. Influence of heat treatments on composition and microstructure

XRD acquisitions were performed after heat treatments lasting from 5 h at 1200°C to 84 h at 1500°C and

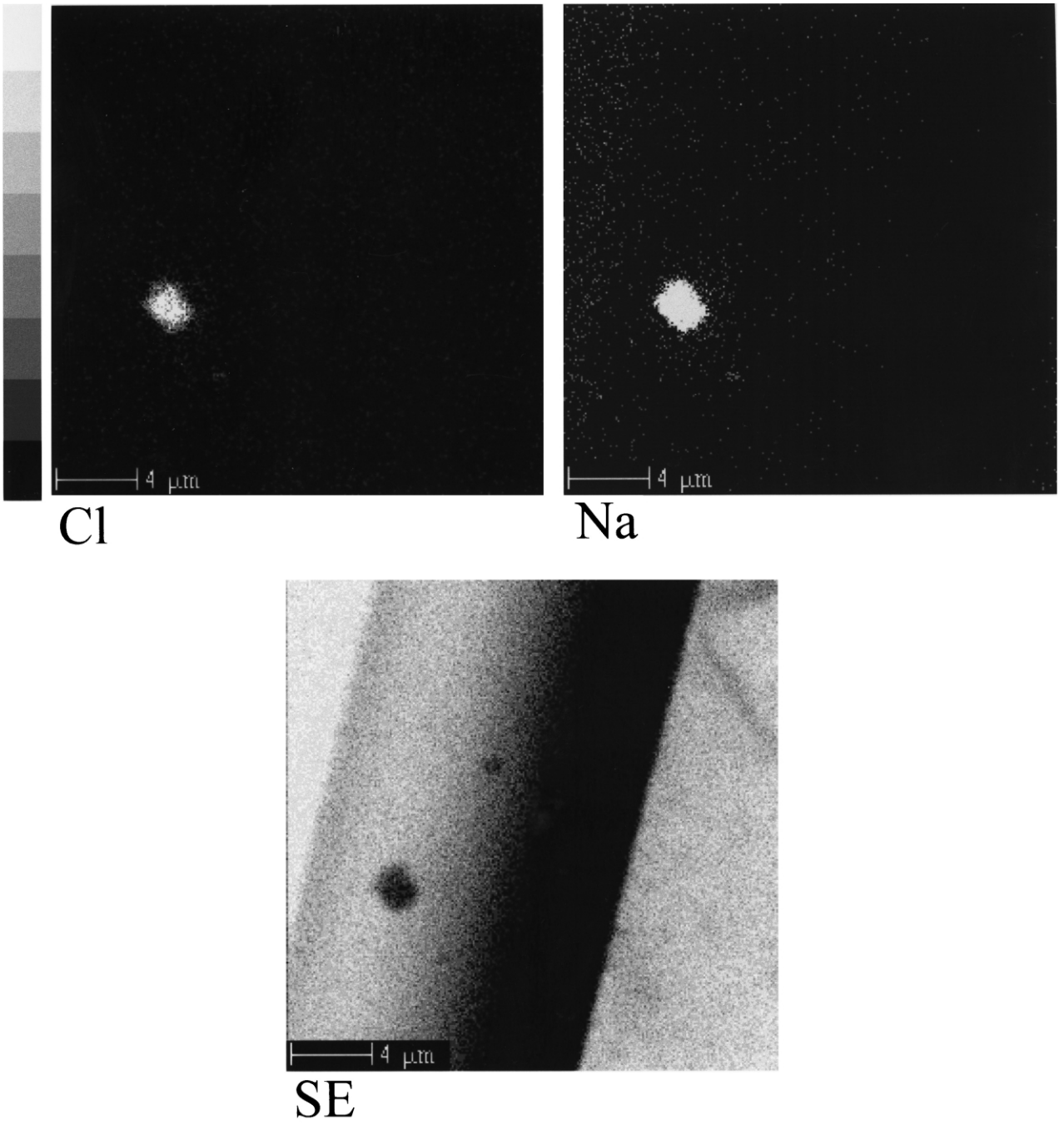

Fig. 3. WDS Cl and Na elemental mapping and corresponding secondary electron image of the fibre surface showing a chlorine and sodium rich inclusion at the fibre surface.

the positions of some peaks are shown in Table 1. From 1200°C, the 210/120 420/240, 041/401 peaks of the mullite were split and the α-alumina peaks increased. Fig. 2 shows the splitting of the mullite peaks 210/120 after a heat treatment of 84 h at 1500°C as well as the increase of the α-alumina peak $01\bar{1}2$ and the set of mullite peaks corresponds to those of the orthorhombic stoichiometric 3:2 mullite.

The evolution of the microstructure after heat treatment was followed by TEM (see Figs. 9–13). During heat treatments the mullite aggregates which contained α-alumina recrystallised into α-alumina-free faceted mullite grains. These mullite grains were smaller than the mullite aggregates as they had rejected the α-alumina particles. Simultaneously the α-alumina grains increased in size leading to the preferential growth of some elongated grains and after 10 days at 1300°C two populations of elongated grains were observed. Table 2 gives the proportions and sizes of the different constituents in the fibre as the function of temperature and duration of heat treatments.

After heat-treatments above 1200°C some fibres showed localised surface defects composed of large α-alumina grains in the form of platelets as can be seen on Fig. 14.

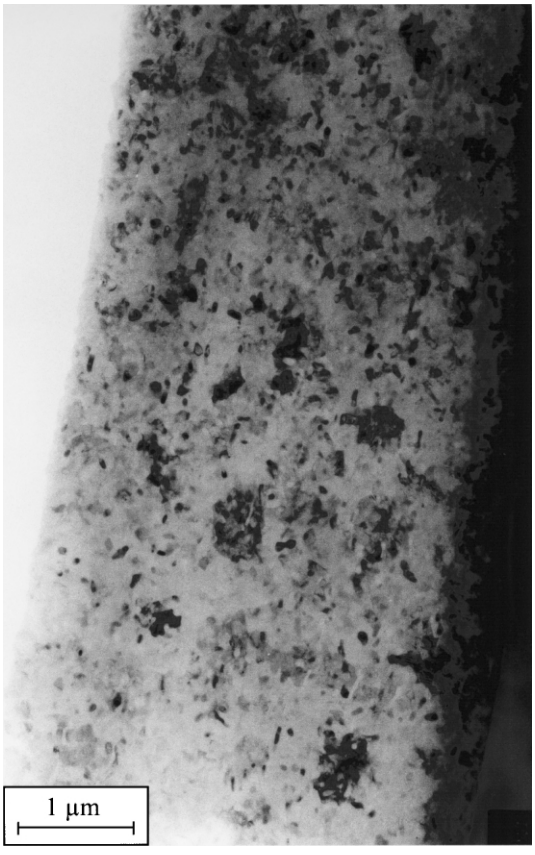

Fig. 4. Microstructure of the as-received fibre revealing mullite aggregates and elongated α-alumina grains.

4.3. Room temperature mechanical properties of as received fibres

Tensile properties of monofilaments were measured at six gauge lengths, between 5 and 250 mm. Thirty filaments were tested at each gauge length. There was no influence of the stress rates on the mechanical properties at room temperature. Table 3 and Fig. 15 summarize the results obtained.

The mean tensile strength was seen to increase with the decrease of the gauge length whereas the Young's modulus was almost constant with a mean value of 251 GPa. Failure strains never exceeded 1%, however, they were superior to those of the FP pure α-alumina fibre.[5]

The fibres showed linear elastic behaviour with brittle failure. The fracture surfaces of all fibres broken at room temperature had a planar appearance and suggested a

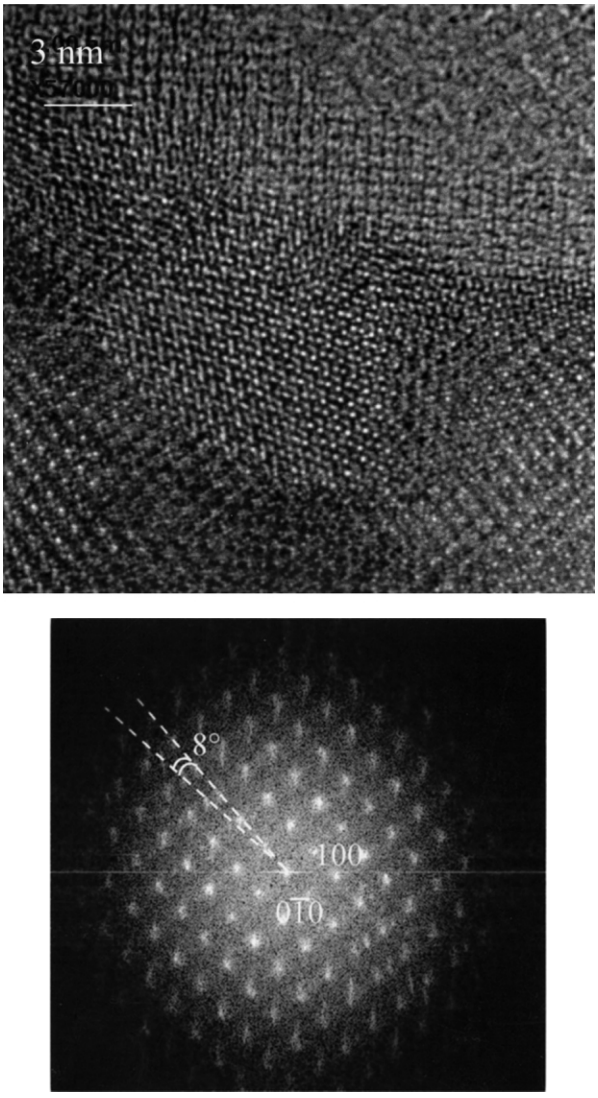

Fig. 5. High resolution image of a mullite aggregate and associated computer generated diffraction pattern obtained by Fourier Transformation (FT) showing a desorientation of 8° between two [010]*.

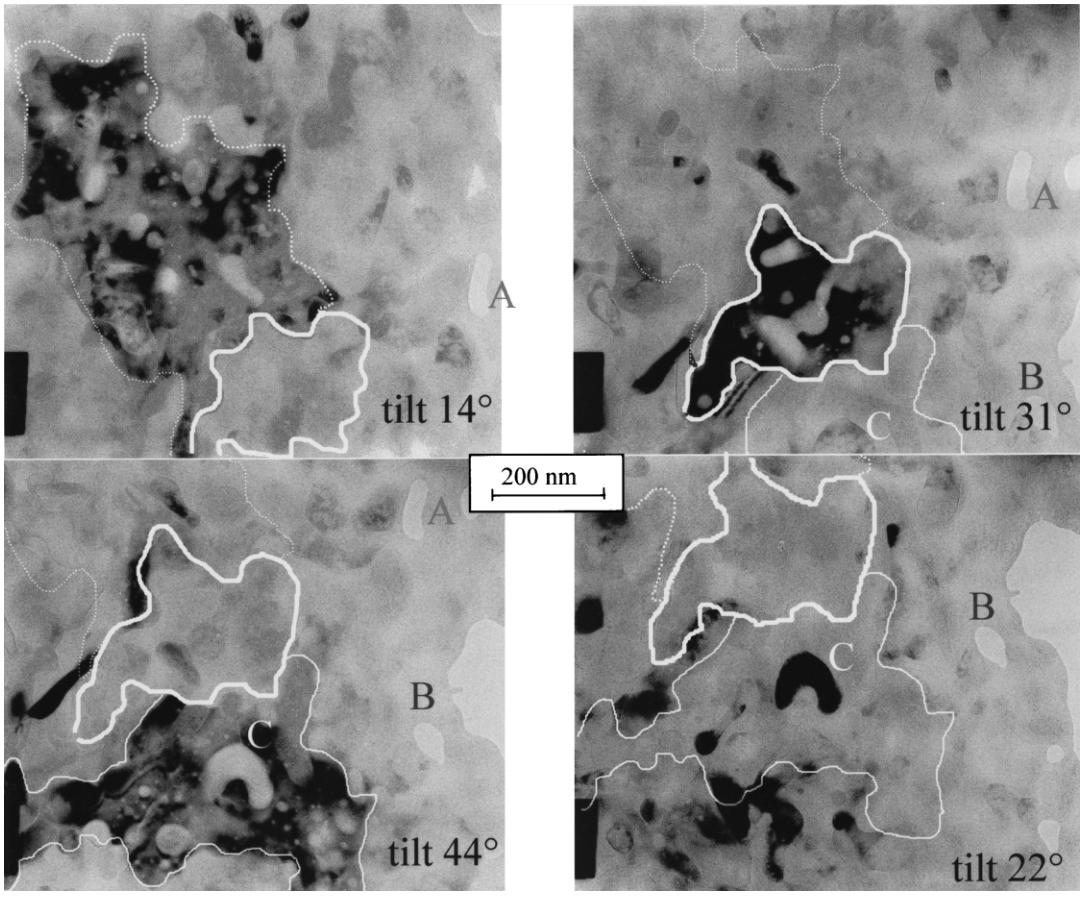

Fig. 6. The same area of the fibre at different angles of tilt showing 3 touching aggregates.

Table 2
Evolution of the proportions and average sizes (in nm) of the different constituents of the as received fibre and after different heat treatments. The maximum and minimum sizes are given when necessary

		Mullite				α-Al_2O_3		
		Aggregate		Facetted grains		Elongated		
		Proportion	Size	Proportion	Size	1st Population	2nd Population	Spherical Size
As-received		100%	300×500	None		100 (from 50 to 300)	None	50 (from 5 to 100)
1200°C	10 days	100%	300×500	None		130 (from 50 to 300)	None	70 (from 20 to 100)
1300°C	5 h	80%	300×500	20%	250	140 (from 50 to 350)	None	70 (from 20)
	10 days	40%	300×500	60%	270	180 (from 80)	A few to 620	100 (from 40)
1400°C	5 h	60%	300×500	40%	250	200 (from 80)	A few to 450	70 (from 30)
	1 day	10%	300×500	90%	300	200 (from 100)	500 (to 650)	100 (from 50)
	4 days	None		100%	500 (up to 1000)	250 (from 70)	1000 (to 1800)	180 (from 50)
1500°C	84 h	None		100%	1000	400 (from 200)	2000 (to >4000)	500

mixed fracture. Fig. 1 shows a failure surface of an as-received N720 broken at room temperature from a surface defect with a failure strength of 1.40 GPa.

4.4. Influence of heat treatments on the mechanical properties

Tensile strengths were measured after different heat treatments and are shown in Fig. 16. Heat treatments of 5 h at temperatures up to 1400°C had no influence on the tensile strength at room temperature. Longer heat treatment at temperatures above 1400°C produced a marked influence on the tensile strength and the room temperature tensile strength dropped by 45% after heat treatment for 4 days at 1400°C.

The Young's modulus increased by about 10% after heat treatment for 5 h at 1200°C as can be seen from Fig. 17. After a heat treatment for 24 h at 1400°C the Young's modulus increased by 19% and was equal to 298 GPa.

The mechanical properties after the heat-treatments at 1500°C for 5 h could not be measured as the fibres were too brittle to be tested.

Fig. 18 shows the fracture morphology of a fibre broken after heat treatment for 24 h at 1200°C. It can be seen that failure was initiated by a large defect, of 1.5 μm, which had developed at the surface. A close examination of the defect shows exaggerated grain growth embedded in a smooth second phase suggesting the presence of an amorphous silicate phase.

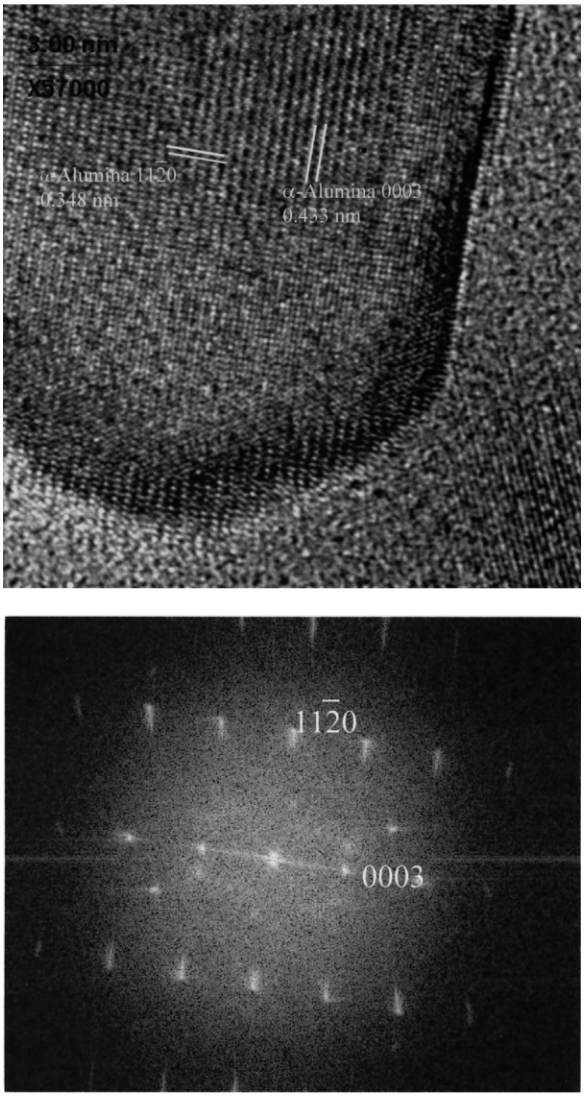

Fig. 7. High resolution image and associated FT image of an α-alumina grain enclosed in mullite revealing that its long facet corresponds to the basal plane.

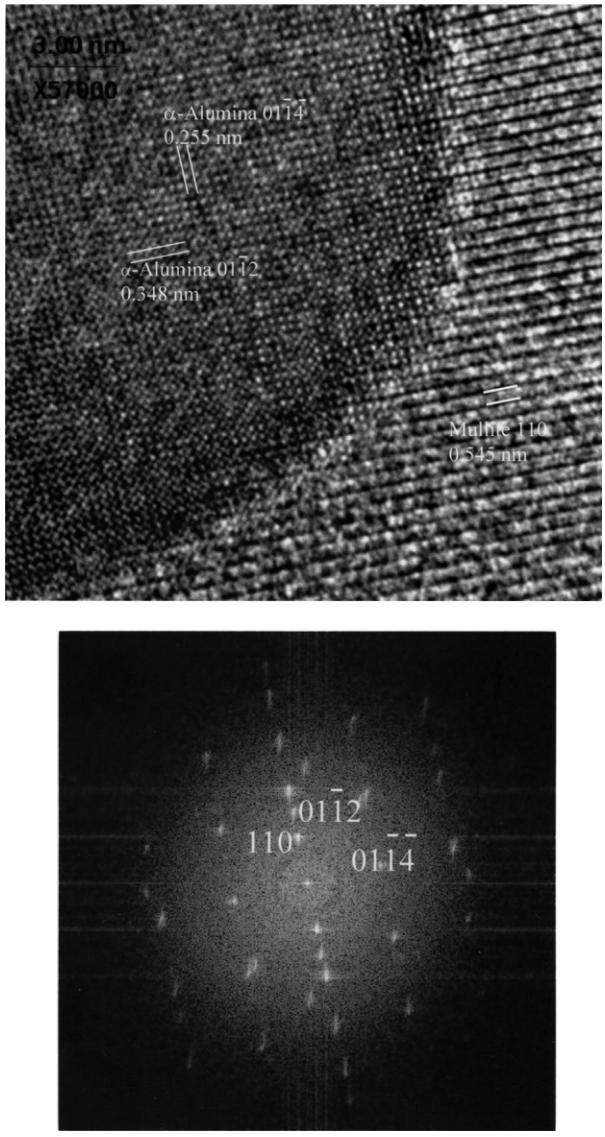

Fig. 8. High resolution image and associated FT image of an α-alumina grain enclosed in mullite, showing that the $\{01\text{-}22\}_{Al_2O_3}$ and $\{110\}_{mullite}$ planes are parallel.

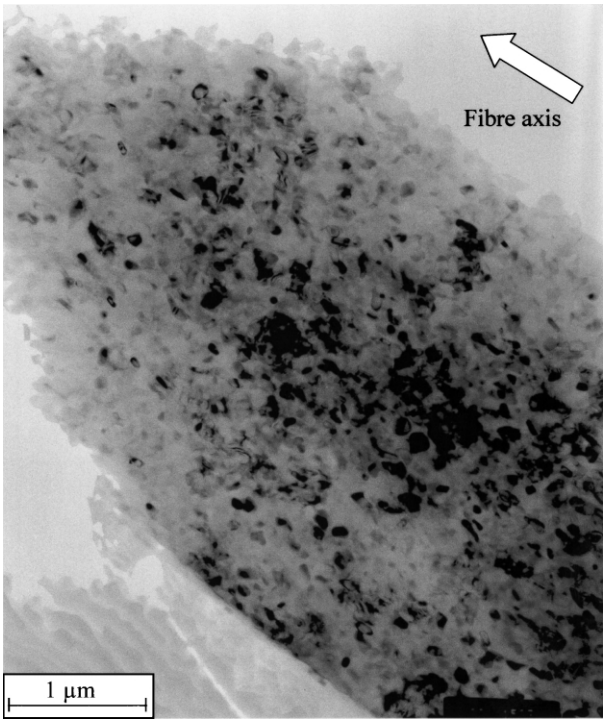

Fig. 9. Microstructure after heat-treatment at 1200°C for 10 days.

Fig. 11. Microstructure after heat-treatment at 1400°C for 24 h.

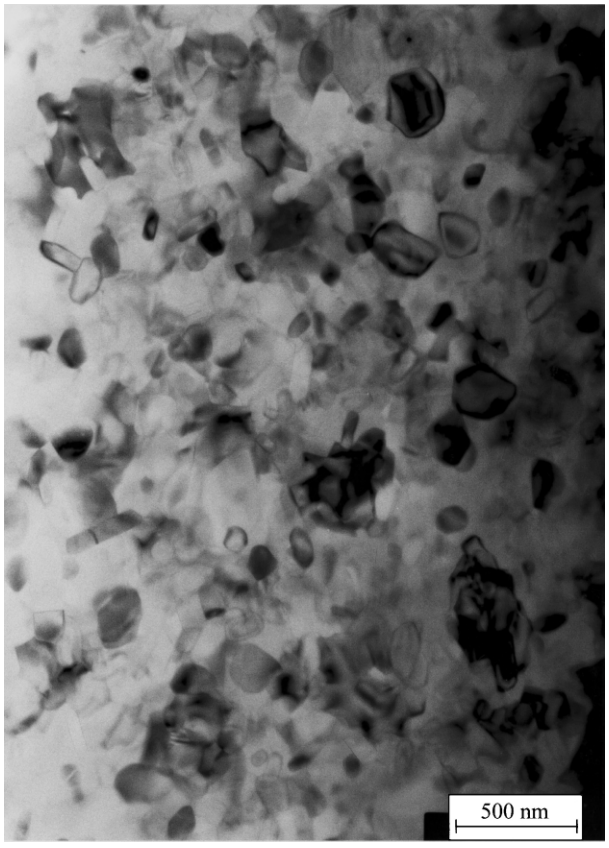

Fig. 10. Microstructure after heat-treatment at 1300°C for 10 days revealing the presence of faceted mullite grains and the bimodal size distribution of α-alumina grains.

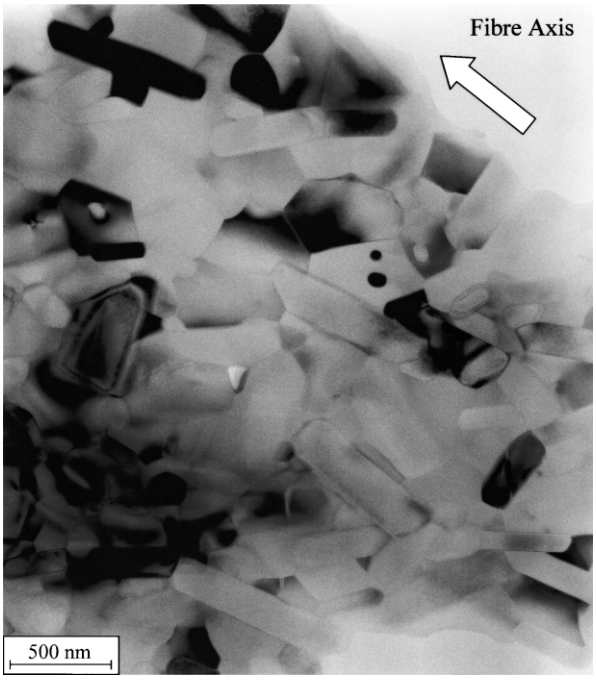

Fig. 12. Microstructure after heat-treatment at 1400°C for 4 days.

5. Discussion

5.1. Microstructure of the as received fibre

The Nextel 720 fibre is composed of a continuum of mullite aggregates of around 500 nm, as illustrated schematically in Fig. 19. Each aggregate is formed of several smaller mullite grains slightly disoriented with respect to each other and which enclose small round or elongated α-alumina grains. It has been shown that, during pyrolysis, α-alumina grains, seeded by iron compounds, crystallise before the mullite grains.[6] The crystallisation of mullite must occur from and around the α-alumina grains as shown by the orientation relationships found between the alumina and mullite grains. The partial orientation of the elongated alumina grains toward the fibre axis results from some orientation of the alumina precursor particles in the sol during fibre spinning.

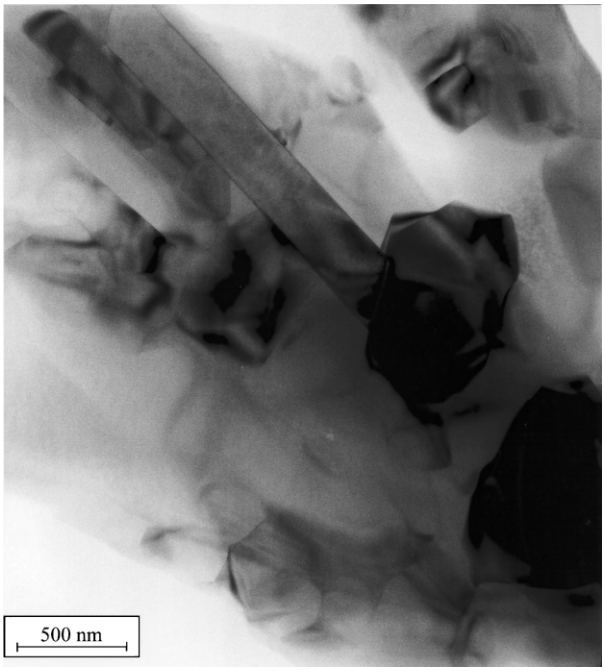

Fig. 13. Microstructure after heat-treatment at 1500°C for 84 h.

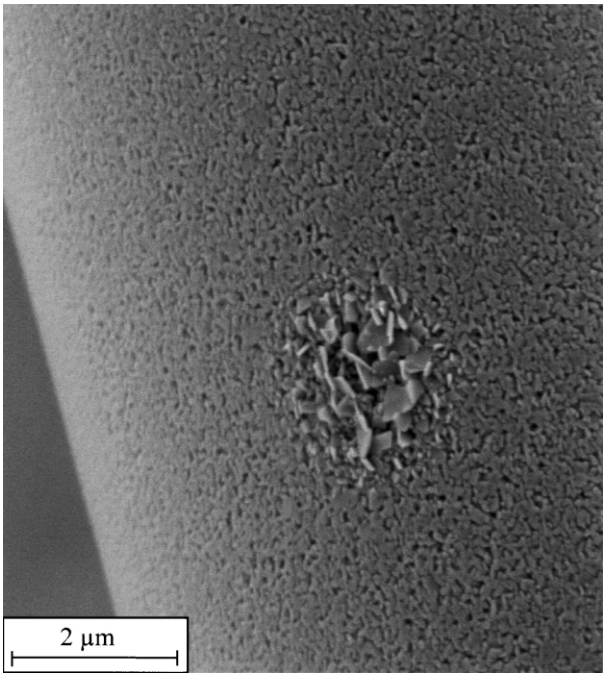

Fig. 14. Local growth of α-alumina platelets in the fibre surface after heat-treatment at 1300°C for 3 h.

Table 3
Room temperature tensile properties and standard deviations for different gauge lengths

Gauge length (mm)	Tensile strength (GPa)	Failure strain (%)	Young modulus (GPa)
250	1.30±0.29	0.52±0.13	249±14
100	1.55±0.27	0.62±0.10	250±10
50	1.62±0.33	0.67±0.12	255±11
25	1.68±0.39	0.66±0.16	252±09
10	1.90±0.38	0.81±0.18	256±27
5	1.92±0.48	0.95±0.24	243±09

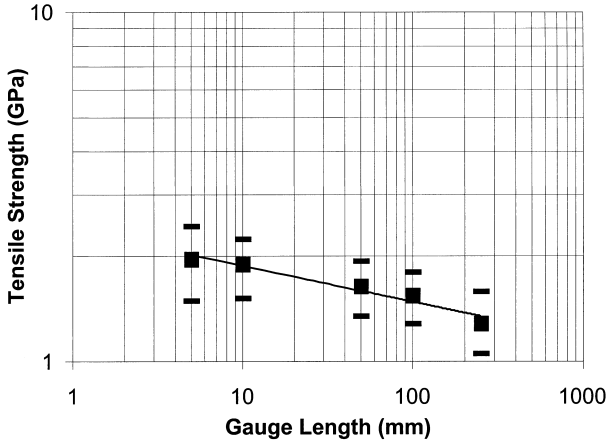

Fig. 15. Tensile strengths of as-received fibre as a function of the gauge length.

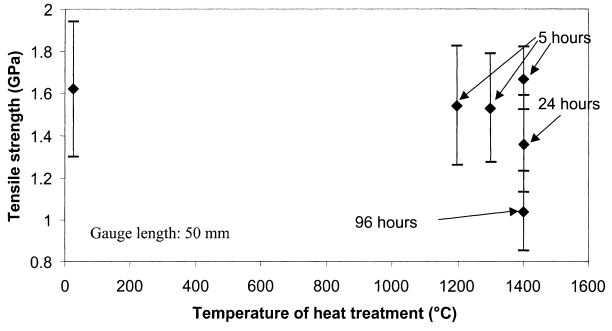

Fig. 16. Tensile strengths after different heat-treatments with a gauge length of 50 mm.

Mullite is the only stable crystalline compound in the Al_2O_3–SiO_2 system under normal atmospheric pressure. It is commonly described as having a composition ranging from $3Al_2O_3{:}2SiO_2$ (60% mol% Al_2O_3) to $2Al_2O_3{:}SiO_2$ (66% mol% Al_2O_3) and crystallising in the orthorhombic system, although compositions from 58 to more than 75 mol% alumina have been reported.[7–11]

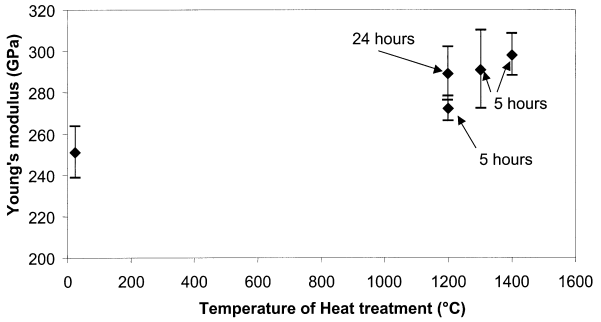

Fig. 17. Evolution of the Young's moduli as a function of heat-treatments.

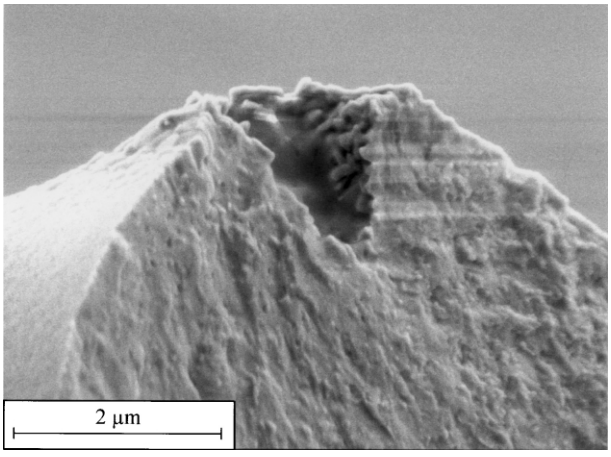

Fig. 18. Fracture surface of a fibre broken at room temperature after heat-treatment for 24 h at 1200°C. A large defect is apparent in which exaggerated grain growth can be seen to have occurred associated with the formation of an amorphous smooth second phase.

In the as received fibre, the hkl and khl mullite peaks are very close to each other indicating that the *a* and *b* cell parameters are almost similar. The symmetry of the mullite is close to pseudo-tetragonal symmetry which has been described by Ossaka and Schneider.[10,11] The cell parameters for the as received fibre and heat treated up to 1400°C were calculated from the positions of the peaks given in Table 4.

The value of the *a* cell parameter is linked to the alumina content *m* in mol% in the mullite by the following relation given by Schneider[11] $m = 144.5a - 1029.5$ where *a* is expressed in Å. This equation allows the alumina content to be calculated in the mullite in the as received fibre which is close to the $2Al_2O_3{:}SiO_2$ mullite as shown in Table 1. The mullite and α-alumina contents by weight in the fibre have then been deduced from the 85 wt.% Al_2O_3 and 15 wt.% SiO_2 composition of the whole fibre. To calculate the volume composition, the density of the mullite has been determined from the

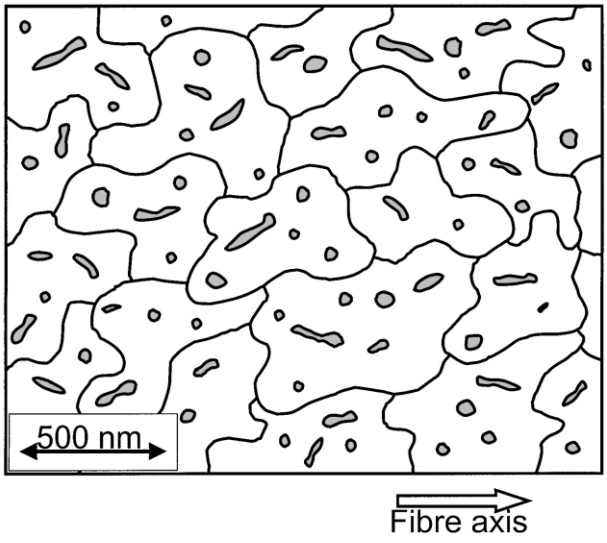

Fig. 19. Schematic representation of the microstructure of the as-received fibre.

Table 4
Alumina content in the mullite phase and the percentage of α-alumina, mullite and porosity in the fibre as a function of heat treatments

		As-received	1200°C 5 h	1400°C 24 h	1500°C 84 h
Mullite cell parameters	a (Å)	7.57	7.54	7.52	7.51
	b (Å)	7.64	7.63	7.65	7.65
	c (Å)	2.88	2.88	2.88	2.87
Alumina content in mullite (m)	(mol%)	64	61	58	56
Mullite content in the fibre	(wt.%/vol.%)	60/66	54/60	50/55	47/52
α-Alumina content in the fibre	(wt.%/vol.%)	40/34	46/40	50/45	53/48
Calculated x		0.34	0.26	0.20	0.14
Calculated density		3.17	3.21	3.21	3.24
Measured Young's modulus	GPa	251 (12)	272 (6)	298 (13)	Not measured
Calculated Young's modulus	GPa	281	291	302	Not measured
Porosity	(%)	5.8	3.4	0.7	Not measured

chemical formula of the average mullite unit cell: $Al_2^{VI}(Al_{2+2x}^{IV}\ Si_{2-2_x}^{IV})O_{10-x}$ where x is the number of oxygen vacancies per average cell. x has been empirically related to m: $x = 10-6\frac{m+200}{m+100}$.[11] The amount of porosity inside the fibre has been evaluated by comparing the measured Young's modulus $E_{exp} = 251$ GPa to the value E_{cal} that can be predicted from a dense uniformly distributed two-phase microstructure using the Paul's semi-empirical expression,

$$E_{cal} = \frac{E_{Al_2O_3}^2 + \left(E_{Al_2O_3}E_{mullite} - E_{Al2O3}^2\right)V_{mullite}^{2/3}}{E_{Al_2O_3} + \left(E_{mullite} - E_{Al_2O_3}\right)V_{mullite}^{2/3}\left(1 - V_{mullite}^{1/3}\right)}$$
$$= 283\ \text{GPa}$$

where the stiffnesses and volume fractions of the two phases are $E_{Al_2O_3} = 400$ GPa, $E_{mul} = 230$ GPa, $V_{Al_2O_3} = 34$, $V_{mullite} = 66$. The values of E_{exp} and E_{cal} are linked to the fraction of porosity, p, by the Mackenzy relationship[12]

$$E_{exp} = E\text{calc} \times \left(1 - 1.9p + 0.8p^2\right)$$

A value of 6.1% in vol has then been calculated for the porosity in the as received Nextel 720 fibre. Finally the as received fibre is composed of 62 wt.% of aggregates of a metastable pseudo-tetragonal 2:1 mullite enclosing 38 wt.% α-alumina and around 6 vol.% porosity.

5.2. Evolution of the microstructure at high temperature

During its fabrication the Nextel 720 fibre is pyrolysed at a temperature lower than 1400°C for a very short time which does not allow the microstructure to be stabilised. Pseudo-tetragonal mullite has been described as being metastable, and transforming gradually to a mullite with a lower alumina content from 1000°C.[13] Heat treatments of the Nextel 720 fibre from 1200 to 1500°C induced a progressive increase in the splitting of the hkl and khl peaks in XRD due to a continuous decrease of a and an increase of b. This evolution of the mullite structure is coupled with a rejection of alumina from the mullite and led to an enrichment in α-alumina in the fibre and an increase in the room temperature fibre stiffness. The values shown in Table 1, which have been calculated by the same method as for the as received fibre, indicate that after a heat treatment at 1500°C for 84 h, the mullite has a silica rich composition, higher than that of the 3:2 mullite. The amount of porosity in the heat treated fibres has been calculated assuming that the fibre is only composed of mullite and α-alumina and does not enclose a significant amount of silica. No clear evidence for the presence of a silicate phase has been found from the TEM observations at room temperature of the heat treated fibres. However, the observed growth of large elongated α-alumina grains from 1300°C and the presence of alkalis in the fibre are indications that a silicate phase has been formed at high temperature. The growth of elongated grains along the dense (0001) planes has been reported [14] to be strongly enhanced by an intergranular liquid phase. Silicate phases with low melting points can be found in the ternary diagrams Na_2O–Al_2O_3–SiO_2 or CaO–Al_2O_3–SiO_2. The Na_2O–Al_2O_3–SiO_2 ternary diagram shows the occurrence of a liquid phase from 1050°C for silica rich mullites in the presence of sodium. It has also been shown[15,16] that the 3:2 mullite can partially dissociate into alumina and silica in the presence of alkalis. The Nextel 720 fibre heated at 1300°C and to higher temperatures is assumed to enclose mullite, α-alumina, and a liquid silicate intergranular phase. The dewetting of the grain boundaries by the silicate phase during cooling explains that no intergranular amorphous phase was observed at room temperature in TEM.

5.3. Nature and distribution of the defects in the fibre

The material did not show strength degradation at temperatures up to 1000°C and the mechanisms of failure were those of a brittle material. Fracture initiated either at a surface or a subsurface defect. The fracture surface morphology was smooth and corresponded to a mixed fracture.

5.3.1. Weibull modulus

To model the failure probability P_R of a fibre of diameter D and length L_o under an applied stress σ_R, with a surface distribution of defects, a unimodal Weibull distribution, was chosen, given by

$$P_R(\sigma_R L_0, D) = 1 - \exp\left[-\left(\frac{\sigma_R}{\sigma_0}\right)^m \cdot L_0 \cdot \pi \cdot D\right]$$

where m is the Weibull modulus, which characterizes the dispersion of the size of the defects in the fibre and σ_0 being the characteristic strength.

The precision in the estimation of the parameter m is directly connected to the number of fibres taken into account in the experimental cumulative failure probability function to be fitted.[17,18] The Weibull expression clearly indicates that the probability of failure varies as a function of stress and surface area and therefore permits the analysis of all the results, grouped together, from all specimens at all gauge lengths and sections. It, therefore, becomes possible to increase the precision for the determination of m by examining all 180 results of the tensile tests at the 6 gauge lengths, plotted on the same curve, by introducing an effective failure stress σ_e expressed as

$$\sigma_e = \sigma_R \cdot (L_0 \cdot \pi \cdot D)^{1/m}$$

The sections of the tested fibres had to be measured prior to each tensile test, due to variations of the fibre diameter within a bundle. The cumulative failure probability was then written as

$$P_R(\sigma_e) = 1 - \exp\left(-\left(\frac{\sigma_e}{\sigma_0}\right)^m\right)$$

where the value of σ_e depends on the value of m which is sought. This value is estimated by an iterative calculation and in this study 25 values of m, ranging from 2 to 8 with steps of 0.25 were examined. For each m, the value of σ_0 was determined to give the best fit between the experimental and the theoretical distributions of failure probability. The appropriateness of the fit was estimated by a Kolmogorov–Smirnov criterion. Among the 25 pairs (m, σ_0) determined by this analysis, the best fit was found for $(m, \alpha_0) = (4.6.2\times10^{-2}$ GPA.m$^{0.5})$. The corresponding experimental and theoretical cumulative functions of failure probability are shown in Fig. 20.

The good agreement between the two curves shows that the Nextel 720 fibre encloses one population of defects, the dispersion in size of which is typical of a brittle material.

5.3.2. Fracture toughness and distribution of the sizes of the defects

The K_{IC} value of the material was calculated from the Griffith's relation applied to a semi-elliptical surface crack measured on Fig. 1. The dimension a_0 of the defect responsible for the failure was measured to be 0.7 μm and the tensile strength was 1.4 GPa.

$$K_{IC} = \sigma Y \sqrt{a_0 \pi}$$

$$\text{with } Y = 0.67^{19} \rightarrow K_{Ic} = 1.4 \text{ MPa}\sqrt{m}$$

Taking this value of K_{Ic} it is possible to calculate the maximum and minimum defect sizes which have provoked failure in the fibres tested at all gauge lengths within the limits defined by the standard deviation. This gives a range of defect sizes from 240 nm to 1.36 μm.

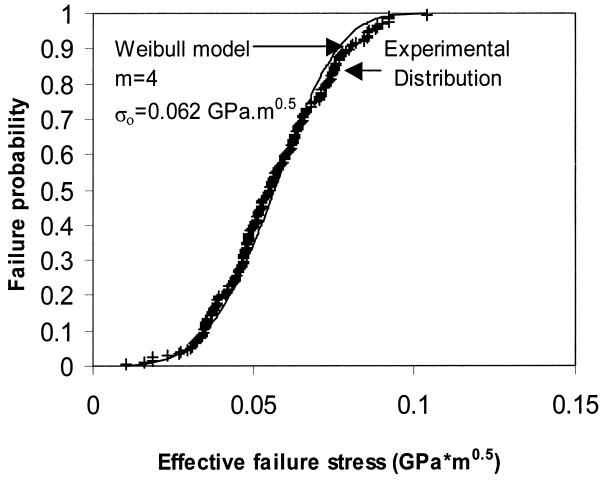

Fig. 20. Failure probability as a function of effective failure stress.

A similar analysis can be made with the results obtained at each gauge length. For example, the defects leading to the failure of a fibre with a gauge length of 50 mm, calculated from the mean failure stress at this gauge length, can be determined to be of 530 nm and if the standard deviation of the stress is taken into account the sizes of the defects range from 370 to 840 nm. The sizes which have been calculated suggest that the defects initiating failure could be due in part to the microstructure at the level of the aggregate boundaries emerging at the fibre surface and also due to surface defects greater than those induced by the microstructure and produced by the manufacturing process.

5.4. Influence of the heat treatment on the mechanical properties

The observation of fracture morphologies together with associated room temperature tensile strengths of fibres which had been heat treated have shown that K_{IC} had not varied.

After heat treatment for 5 h up to 1400°C the mean failure strengths of the fibres obtained at room temperature were found to be unchanged with respect to the as received strength, which was around 1.6 GPa for a gauge length of 50 mm. However after 24 h at 1400°C the fibre strength was found to have decreased to a mean value of 1.36 GPa. A calculation of the defect size gives a value of 750 nm with a range of 540 nm to 2.12 μm. The lower value is correlated to the preferential growth of α-alumina grains observed in the fibre after such heat treatment.

The presence of a silicate phase and the exaggerated grain growth in the largest defects, as shown in Fig. 18 suggest a correlation with the surface spots of alkaline contaminants which have been revealed. As discussed above, these defects are created by the decomposition of the mullite phase in the presence of alkalis. This results in the formation of an alumino-silicate phase which allows the growth of large alpha alumina grains through liquid diffusion. The larger defects must have been created by local chemical heterogeneities at the fibre surface leading to microstructural instability.

6. Conclusion

The microstructure and tensile properties of the as-received and heat-treated Nextel 720 fibre have been studied. The fibres are composed of aggregates of a metastable (≈2:1) mullite in which are embedded α-alumina grains, some of which are elongated. This is due to the brief axposure of the fibre to temperatures below 1400°C during its manufacture. Heat treatments at

temperatures above 1300°C provoke a rearrangement of the structure which evolves toward facetted (3:2) mullite grains and elongated oriented α-alumina grains. This change is accompanied by an increase in Young's modulus and a fall in room temperature strength. The presence of mullite which is inherently resistant to creep and elongated oriented alumina grains which appear after heat treatment suggests that the fibre would posses high resistance to creep.

Acknowledgements

The authors wish to acknowledge the support of the European Commission which has largely financed the study within the BRITE research programme, No BRPRCT95-0110. They also wish to thank U. Dahmen, Director of the NCEM, LBNL, for his hospitality in allowing the high resolution microscopy to be carried out at the University of California for which the help of Ch. Nelson was indispensable. This part of the study was funded by the Office of Energy Research, Office of Basic Energy Sciences, Mat. Sci. Div. of the US D.O.E. under contract No. DE-AC03-76SF00098.

References

1. Wilson, D. M., Lieder, S. L. and Luenburg, D. C., Microstructure and high temperature properties of nextel 720 fibres. *Ceramic Engineering and Science Proceedings*, 1995, **16**(5), 1005–1014.
2. Hagege, R. and Bunsell, A. R., Testing methods for single fibres. In *Fibre Reinforcement for Composite Materials, Vol. 2*, ed: A.R. Bunsell. Elsevier, 1988, pp.479–487.
3. Berger, M. H. and Bunsell, A. R., Thin foil preparation of small diameter ceramic or glass fibres for observation by TEM. *J. Mater. Sci. Lett*., 1993, **12**, 825–828.
4. Bunsell, A. R., Hearle, J. W. S. and Hunter, R. D., An apparatus for fatigue-testing of fibres, *J. Phys. E*., 1971, **4**, 868–872.
5. Lavaste, V., Berger, M. H. and Bunsell, A. R., Microstructure mechanical characteristics of alpha-alumina-based fibres. *J. Mater. Sci*., 1995, **30**, 4215–4225.
6. Wilson, D.M., 3M private communication.
7. Aksay, J. A. and Pask, J. A., Stable and metastable equilibria in the system silica-alumina. *J. Am. Ceram. Soc*., 1975, **58**(11-12), 507–512.
8. Pask, J. A., Importance of starting materials on reactions and phase equilibria in the alumina silica system. *J. Eur. Ceram. Soc*., 1996, **16**, 101–108.
9. Klug, F., Prochazka, S. and Doremus, R. H., Alumina-silica phase diagram in the mullite region. *J. Am. Ceram. Soc*., 1987, **70**(10), 750–759.
10. Ossaka, J., Tetragonal mullite-like phase from co-precipitated gels. *Nature*, 1961, **191**(4792), 1000–1001.
11. Schneider, H. and Rymon-Lipinski, T., Occurence of pseudotetraonal mullite. *J. Am. Ceram. Soc*., 3, **71**, C.162.
12. Mackenzie, J. K., *Proc. Phys. Soc. London*, 1950, **63B**, 2–11.
13. Fischer, R. X., Schneider, H. and Voll, D., Formation of aluminium Rich 9:1 mullite and its transformation to low alumina mullite upon heating. *J. Eur. Ceram. Soc*., 1996, **16**, 109–113.
14. Song et Coble, Morphology of platelike abnormal grains in liquid-phase sintered alumina. *J. Am. Ceram. Soc*., 1990, **73**(7), 2086–2090.
15. Kleebe, H. J., Hilz, G. and Ziegler, G., TEM and EELS characterization of glass phase in sol–gel derived mullite. *J. Am. Ceram. Soc*., 10, **79**, 2592–2600.
16. Baudin, C. and Pilar Villar, M, Influence of thermal aging on microstructural development of mullite containing alkalis. *J. Am. Ceram. Soc*., 1998, **81**(10), 2741–2745.
17. Berdin, C., Cailletaud, G. and Jeulin, D., Estimation of probabilistic brittle fracture models for ceramics. In: Proceedings of the ICASP 7 conference, Paris, France, eds. M. Lemaire, J. L. Favre and A. Mebarki, 1995.
18. Berdin, C., Cailletaud, G. and Jeulin, D., Brittle failure prediction of ceramics using a multiscale approach. *J. Am. Ceram. Soc*., 1996, **79**(11), 2825–2832.
19. *Stress Intensity Factors Handbook*, *Vol. 2*, ed. Y. Murakami, Pergamon Press, 1987, pp. 645–655.